Zdeněk P. Bažant

McCormick Institute Professor and
W.P. Murphy Professor of Civil and Mechanical
Engineering and Materials Science,
Northwestern University,
2145 Sheridan Road,
CEE/A135, Evanston, IL 60208
e-mail: z-bazant@northwestern.edu

Marco Salviato

Postdoctoral Associate
Department of Civil
and Environmental Engineering,
Northwestern University,
2145 Sheridan Road,
Evanston, IL 60208

Viet T. Chau

Research Assistant
Department of Civil
and Environmental Engineering,
Northwestern University,
2145 Sheridan Road,
Evanston, IL 60208

Hari Visnawathan

Subsurface Flow and Transport Team Leader
Computational Earth Science,
EES-16, Sch. A,
Los Alamos National Laboratory,
Los Alamos, NM 87545

Aleksander Zubelewicz

Los Alamos National Laboratory,
Los Alamos, NM 87545

Why Fracking Works

Although spectacular advances in hydraulic fracturing, also known as fracking, have taken place and many aspects are well understood by now, the topology, geometry, and evolution of the crack system remain an enigma and mechanicians wonder: Why fracking works? Fracture mechanics of individual fluid-pressurized cracks has been clarified but the vital problem of stability of interacting hydraulic cracks escaped attention. First, based on the known shale permeability, on the known percentage of gas extraction from shale stratum, and on two key features of the measured gas outflow which are (1) the time to peak flux and (2) the halftime of flux decay, it is shown that the crack spacing must be only about 0.1 m. Attainment of such a small crack spacing requires preventing localization in parallel crack systems. Therefore, attention is subsequently focused on the classical solutions of the critical states of localization instability in a system of cooling or shrinkage cracks. Formulated is a hydrothermal analogy which makes it possible to transfer these solutions to a system of hydraulic cracks. It is concluded that if the hydraulic pressure profile along the cracks can be made almost uniform, with a steep enough pressure drop at the front, the localization instability can be avoided. To achieve this kind of profile, which is essential for obtaining crack systems dense enough to allow gas escape from a significant portion of kerogen-filled nanopores, the pumping rate (corrected for the leak rate) must not be too high and must not be increased too fast. Furthermore, numerical solutions are presented to show that an idealized system of circular equidistant vertical cracks propagating from a horizontal borehole behaves similarly. It is pointed out that one useful role of the proppants, as well as the acids that promote creation of debris in the new cracks, is to partially help to limit crack closings and thus localization. To attain the crack spacing of only 0.1 m, one must imagine formation of hierarchical progressively refined crack systems. Compared to new cracks, the system of pre-existing uncemented natural cracks or joints is shown to be slightly more prone to localization and thus of little help in producing the fine crack spacing required. So, from fracture mechanics viewpoint, what makes fracking work?–the mitigation of fracture localization instabilities. This can also improve efficiency by fracturing more shale. Besides, it is environmentally beneficial, by reducing flowback per m^3 of gas. So is the reduction of seismicity caused by dynamic fracture instabilities (which are more severe in underground CO_2 sequestration). [DOI: 10.1115/1.4028192]

1 Introduction

Hydraulic fracturing of oil and gas bearing rocks, also known as "fracking,"[1] is an established technology [1–5] that has been developed gradually since 1947, with no government support until the success has been proven. Although the recent advances in fracking have been nothing less than astonishing, the knowledge of the actual fracturing process is mostly empirical and makes a mechanician wonder: Why the fracking works?

The intent of this article, based on report [6], is (1) to suggest an explanation in terms of stability of interactive cracks systems, and to (2) present a method to estimate the hydraulic crack spacing from gas flux history observed on the surface, from the known percentage of gas extraction from the shale stratum, and from the known permeability of shale.

Complete analysis will require simulating in detail the diffusion of gas through orthotropic shale, and the flow of gas and water with proppants and gellants through the hierarchical crack system and along the pipes. It will also require the orthotropic constitutive laws for nonlinear triaxial softening damage, quasi-brittle

cohesive fracture, and creep of the shale. Such analysis must be relegated to subsequent studies.

2 An Aperçu of Fracking Technology

The gas bearing stratum of tight shale, usually about 3 km below the surface and 20–150 m in thickness [7,8], is accessed by parallel horizontal boreholes emanating from a single vertical well in the direction of the minimum principal tectonic stress σ_h, whose magnitude is about 1/5 to 4/5 of the overburden stress σ_g [9].

The horizontal boreholes are typically about 500 m apart and several kilometers long. Each of them is subdivided into about five segments, each of which consists of about 5–9 fracturing stages. Each stage, about 70 m long, is further subdivided into about 5–8 perforation clusters. In each cluster, about 14 m long, the steel casing (or pipe), of typical inner diameter 3.5 in. (77 mm) [10,11], is perforated at 5–8 locations by detonating shaped explosive charges (Fig. 1).

Powerful pumps on the surface drillpad inject the fracking fluid into the shale stratum. The fluid, with a proppant (fine sand) mixed into it, is about 99% water and contains various additives, such as gellants, acids, or pH controlling ions. Each stage requires injection of several million gallons of water (which is equivalent to about 1–2 mm of rain over the area of the lease, 3×5 km^2). The flowback of water represents only about 15% of the injected total and is highly contaminated. Strict controls are required to prevent its accidental release to the environment. Often, the water flowback is reinjected underground. Minimization and treatment of this flowback is a paramount objective of technology improvement.

Pumps, currently attaining at the surface level the pressure of about 25 MPa, force the fracking fluid through the perforations

[1]Although this term is often used pejoratively, it is adopted here because of its brevity. If used in science, it will cease to be disparaging.
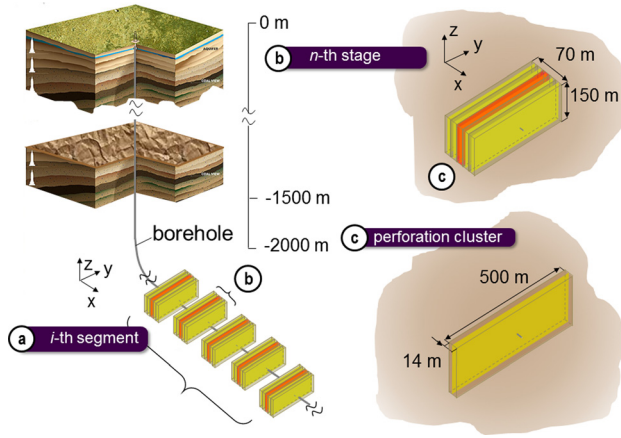
Fig. 1 Overall scheme of hydraulic fracturing: (a) one of many segments, subdivided in 5–8 fracturing stages; (b) one fracturing stage composed of 5–8 pipe perforation cluster; (c) one perforation cluster with 5–8 perforations along the pipes (not to scale)

Fig. 2 Schematic of gas flow from shale to surface, showing a layer of shale between two open vertical hydraulic cracks of spacing s, with subsequent profiles of gas pressure p, and the passage of gas to the surface

into the shale stratum. The shale is intersected by a system of natural fractures or rock joints, nearly vertical, which are either tightly closed or filled by calcite or other minerals. They are typically 15–50 cm apart [5,12]. The shale is also intersected by numerous finer faults and slip planes, and contains weak near-horizontal bedding planes with millimeter spacing, which have higher permeability and higher concentration of kerogen filled nanovoids [13]. The first, large, hydraulically produced cracks must be roughly normal to the horizontal wellbore, since it is always drilled in the direction of the minimum tectonic stress.

3 A Fracture Mechanician's Puzzle

Most of the gas, principally methane, is contained in isolated kerogen-filled nanopores of diameters from 0.5 nm to about 10 nm [13–15]. From drilled cores brought to the surface, the gas content per unit volume of shale is known, and thus it is estimated that only about 15%, and often as little as 5%, of the gas content of the shale stratum gets extracted by the fracking process (percentages as high as 50% have been heard but probably represent local aberration of one fracking stage).

Although this percentage seems low, it is nevertheless a puzzle why the percentage is not orders of magnitude lower, given the extremely low shale permeability, k, and the fact that parallel cracks tend to localize into widely spaced widely opened cracks. To provide an answer, we will first try to figure out from surface gas flux observations the spacing of hydraulic cracks in shale, and then we will discuss how to achieve it.

4 Estimation of Hydraulic Crack Spacing From Observed Gas Outflow History

4.1 Diffusion of Gas Through the Shale Toward the Hydraulic Cracks. The reported values of shale permeability, k, range from 10^{-9} darcy to 10^{-7} darcy (which is 10–1000 times lower than the typical permeability of concrete); e.g., Ref. [16]. The huge spread of the measured k-values reported in the literature [13,17–19] is probably caused less by differences among locations and more by differences among the methods of measurement [20,21]. These are transient methods based on the long-term decay of gas loss using: (1) a drilled core or (2) powderized shale, obtained by grinding to particle size of cca 0.5–0.85 mm.

The core test is dominated by diffusion along the kerogen-filled bedding layers which are far more permeable than the rest, while the powder test is dominated by powder from the compacted clay rock between the bedding layers which are much less permeable
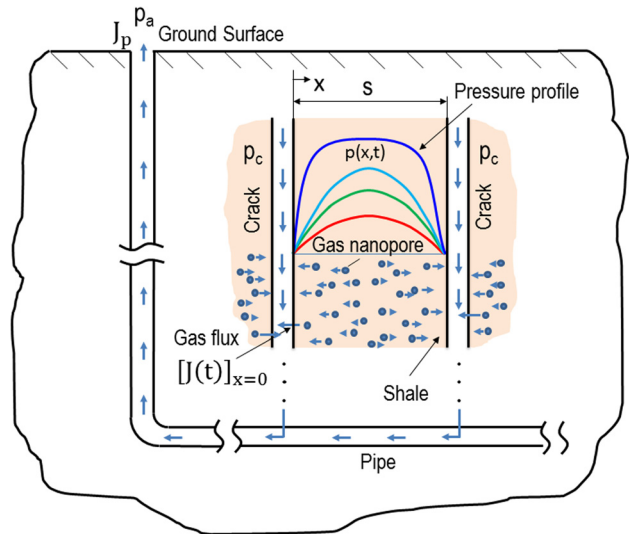
and thus lose their gas much slower. For the hydraulic cracks that are roughly orthogonal to the bedding layers, the core test matters. For cracks parallel to the bedding layers, the powder test matters, although such cracks are probably rare, due to overburden pressure. We will consider both extreme cases but a mixture of both is sure to occur in fracking. Thus the average permeability, 10^{-8} darcy, may be most relevant and is here used in calculations.

The first question is: How does the gas escape from the nanovoids into the nearest cracks? As a typical situation, consider one-dimensional gas diffusion in direction x into adjacent parallel cracks of spacing s, normal to x (Fig. 2). The Darcy law is assumed to apply, i.e.,

$$v = -\frac{k}{\mu}\frac{\partial p}{\partial x} \tag{1}$$

where v = effective velocity of gas, p = gas pressure, and μ = dynamic viscosity. Mass conservation requires that

$$\frac{\partial(\phi\rho)}{\partial t} + \frac{\partial(\rho v)}{\partial x} = 0 \tag{2}$$

where t = time, ϕ = gas porosity, μ = dynamic viscosity of the gas [4,22], and C_s = bulk compressibility of shale; ρ = mass density of gas, which is assumed to behave as ideal gas, i.e., $p/\rho = RT$ = const. It follows that the gas compressibility $C_g = 1/p$. Substituting $p = \rho RT$ and Eq. (1) into Eq. (2) and noting that constant RT cancels out, we get, after rearrangements,

$$\frac{\phi\mu}{k}\left(C_s + \frac{1}{p}\right)\frac{\partial p}{\partial t} = \frac{1}{p}\frac{\partial}{\partial x}\left(p\frac{\partial p}{\partial x}\right) \tag{3}$$

This well-known diffusion equation [23] is nonlinear. The nonlinearity is caused by the dependence of gas compressibility on p.

Consider now a shale layer between two parallel cracks at $x = 0$ and $x = s$. The flux of gas from the shale layer into the cracks at $x = 0$ is

$$J = -\frac{\rho k}{\mu}\left[\frac{\partial p}{\partial x}\right]_{x=0} \tag{4}$$

This represents an interface condition for the flow of gas into the hydraulic crack system. With this interface condition, Eq. (3) is solved numerically by central finite differences in the x direction and explicit finite forward steps Δt in time. The steps are increased, within the stability limit, as the rate of diffusion decays.

4.2 Crack Volume and Total Surface Area of Hydraulic Cracks.

Next we need to attempt a crude estimate of the mass flux of gas observed at the surface drillpad. For that we need to estimate the total volume V_c and total surface area S_c of all the hydraulic cracks in a fracturing stage. The basic question is: What is the shale volume that gets fractured?

The answer can be deduced based on the fact that the percentage γ_g of gas extracted from the shale stratum is known; optimistically we consider $\gamma_g = 15\%$. In this regard consider two simple possibilities:

(1) the 15% gas extraction occurs uniformly throughout the stratum or
(2) the gas extraction eventually becomes almost complete but occurs within only 15% of the volume of shale stratum.

If the former was true then, at the end of operation of the well, the rate of gas flow would still be very high, roughly about 68% of the peak value. Obviously such a well would not be abandoned. Therefore, the latter must be the case.

The fracking stage length along the horizontal pipe is considered as $L_x = 70$, the height of the fracked zone as $L_z = 150$ m (which is about the maximum, though apparently very frequently encountered, thickness H of the shale stratum), and the width as $L_y = 400$ m (Fig. 3). Since the fracking pressure only rarely exceeds the overburden pressure, we consider that all the cracks (with spacing s yet to be estimated) are vertical, the first system of cracks approximately orthogonal to the direction of the tectonic stress of minimum magnitude, and the second system of vertical cracks approximately orthogonal to the first.

To make analytical estimates possible, we consider the fracked zone to be an elliptical cylinder with a vertical axis, height h, and a generating horizontal ellipse of axes a and b (Fig. 3(a)). If this cylinder occupied the full height H of the stratum, we would have $h = H = 150$ m. But, as argued, we must shrink the volume of this elliptical cylinder to 15%, which we do by scaling all the dimensions in equal ratio, which is $0.15^{1/3} = 0.531$. Thus $a = 0.15^{1/3} L_y/2 = 106.3$ m, $b = 0.15^{1/3} L_x/2 = 18.6$ m, and $h = 0.15^{1/3} H = 79.7$ m. The volume of the shrunken zone, which is $V_Z = \pi abh = 494{,}801$ m³, is assumed to be intersected by vertical cracks on a square horizontal grid (Fig. 3(b)) of spacing s. The total surface area of such cracks (each crack having two faces) is $S_c = 4\pi abh/s = \pi L_x L_y h/s$. For irregular crack systems, one may take $s = V/S_c$ where $V =$ cracked shale volume.

To estimate the volume of the opened cracks, we first calculate the enlargement of the area of the idealized ellipse considered as a
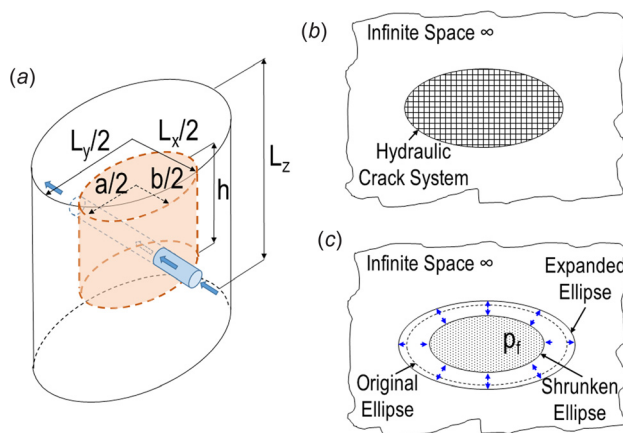

Fig. 3 Schematic of (a) the volume of shale stratum to be fracked, considered for the purpose of analysis as elliptical cylinder, and a scaled-down cylinder representing the portion of shale volume that is actually fracked; (b) undeformed and (c) deformed cross sections of the scaled cylinder, reduced according to the known percentage of terminal gas extraction from the shale

hole in an infinite elastic plane with elastic modulus $E = 37.5$ GPa and Poisson ratio $\nu = 0.3$, which is typical of the shale properties along the bedding layers. By extending the complex potential analysis, as presented in Ref. [24], to displacements, the area increase ΔA of the elliptical hole in infinite plane due to internal fracking pressure p_f (considered to be in excess of the average remote tectonic pressure $p_{tectonic} = (\sigma_h + \sigma_H)/2 \approx 40$ MPa) has been calculated as $\Delta A = 2.04 p_f$; see the Appendix. Assuming for simplicity the same area increase at all horizontal sections of the elliptical cylinder, one gets the volume increase $\Delta V_1 = L_z \Delta A$. This is an estimate of the contribution of the compression of the surrounding shale to the total volume of all opened cracks.

Another contribution is due to the compression of the shale between the cracks (Fig. 3(c)). Since on each horizontal plane the elliptical cross section is under biaxial pressure p_c, equal to the fracking pressure $p_f \approx 5$ MPa (in excess of the original tectonic pressure), the contribution of the shale contraction to the crack volume is $\Delta V_2 = \pi ab L_z p_f/E_p$ where $E_p = E/2(1 - \nu)$ for plane stress. The total volume of the opened vertical cracks of both orientations is thus estimated as $\Delta V_c = \Delta V_1 + \Delta V_2$. With the aforementioned input values, one finds that $\Delta V_c = 907$ m³, which is 0.18% of the total volume $V_Z = 494{,}801$ m³.

4.3 Transport of Gas From Hydraulic Crack System to Surface Drillpad.

To estimate s, we need to figure out the rate of gas flow through the hydraulic cracks and through the horizontal and vertical pipes. Since the gas is mostly methane and methane does not dissolve in water, the gas must move as bubbles, which start as microscopic but soon coalesce into big bubbles filling the crack thickness and the pipe diameter. In the hydraulic crack system, as well as in the horizontal and vertical pipes, the bubbles are driven by gas pressure gradient and move in turbulent flow. In the vertical pipe, the movement of gas bubbles is, additionally, also propelled gravitationally by buoyancy.

Modeling of the movement of gas bubbles is very complicated and its details are neglected here. For the present purpose, it should suffice to use the Hagen–Poiseuille law for flow of a compressible fluid in pipes

$$J_p = -\frac{\rho b_1}{\mu L}\left(\frac{p_c^2 - p_a^2}{p_a}\right) \tag{5}$$

where $J_p =$ flux of gas out of the fracked zone; $p_c =$ inlet pressure = gas pressure at, approximately, the center of the fracked zone; $p_a =$ atmospheric pressure = gas pressure at exit on the surface; $L =$ distance of flow; and $b_1 =$ constant characterizing the resistance to gas flow through the hydraulic crack system and the horizontal and vertical sections of the pipe.

To complete the gas transfer model we need the condition of mass balance of gas within the hydraulic crack system. Since the rate of change of mass m_c of gas contained in all the opened hydraulic cracks is $dm_c/dt = J_p - A_c J$, the mass balance condition may be approximated as

$$J_p - A_c J = \rho V_c C_g \frac{dp_c}{dt}, \quad C_g = \frac{1}{p_c} \tag{6}$$

where $p_c =$ average gas pressure in the crack system, $C_g =$ gas compressibility, $V_c =$ total volume of the opened hydraulic cracks, $A_c =$ area of the surfaces of all opened hydraulic cracks ($=$ double of the total crack area, S_c, because each crack has two surfaces from which gas streams into the crack).

Subtracting Eqs. (5) and (6) and expressing J from Eq. (4), we obtain the final approximate equation for the decay of gas pressure p_c in the hydraulic crack system

$$\frac{dp_c}{dt} + \frac{p_c}{\tau}\frac{p_c^2 - p_a^2}{p_a^2} = \frac{A_1 k}{\mu}p_c\left[\frac{\partial p}{\partial x}\right]_{x=0} \tag{7}$$

in which

$$\tau = L V_c \mu/b_1 p_a, \quad A_1 = A_c/V_c \tag{8}$$

4.4 Crack Spacing and Halftime Optimally Matching Observations, and Their Errors. Figures 4(a) and 4(b) show five histories of gas flux at the surface observed at five different wells in Fayettville shale in Arkansas (posted on the web) [25]. The histories are plotted in actual time scale on the left and the logarithmic time scale on the right. They have two key features that must be matched by computations:

(1) the time, τ_{peak}, in which the peak flow is reached
(2) the rate of postpeak flux decay

Matching these two times makes it possible to estimate two key unknowns—spacing s and halftime τ, τ (at which the peak rate drops not to a half but to about $0.2 J_p(\tau_{peak})$).

The foregoing formulation has been programmed and the histories in Fig. 4(a) were matched as shown by the smooth solid curve. This match provides the average optimum estimates

$$s = s_{opt} = 0.1 \text{ m}, \quad \tau = \tau_{opt} = 26 \text{ months} \quad (9)$$

Aside form the input data already mentioned, further input data were: fluid viscosity, $\mu = 1.35 \times 10^{-5}$ Pa s, porosity $\phi = 0.1$,
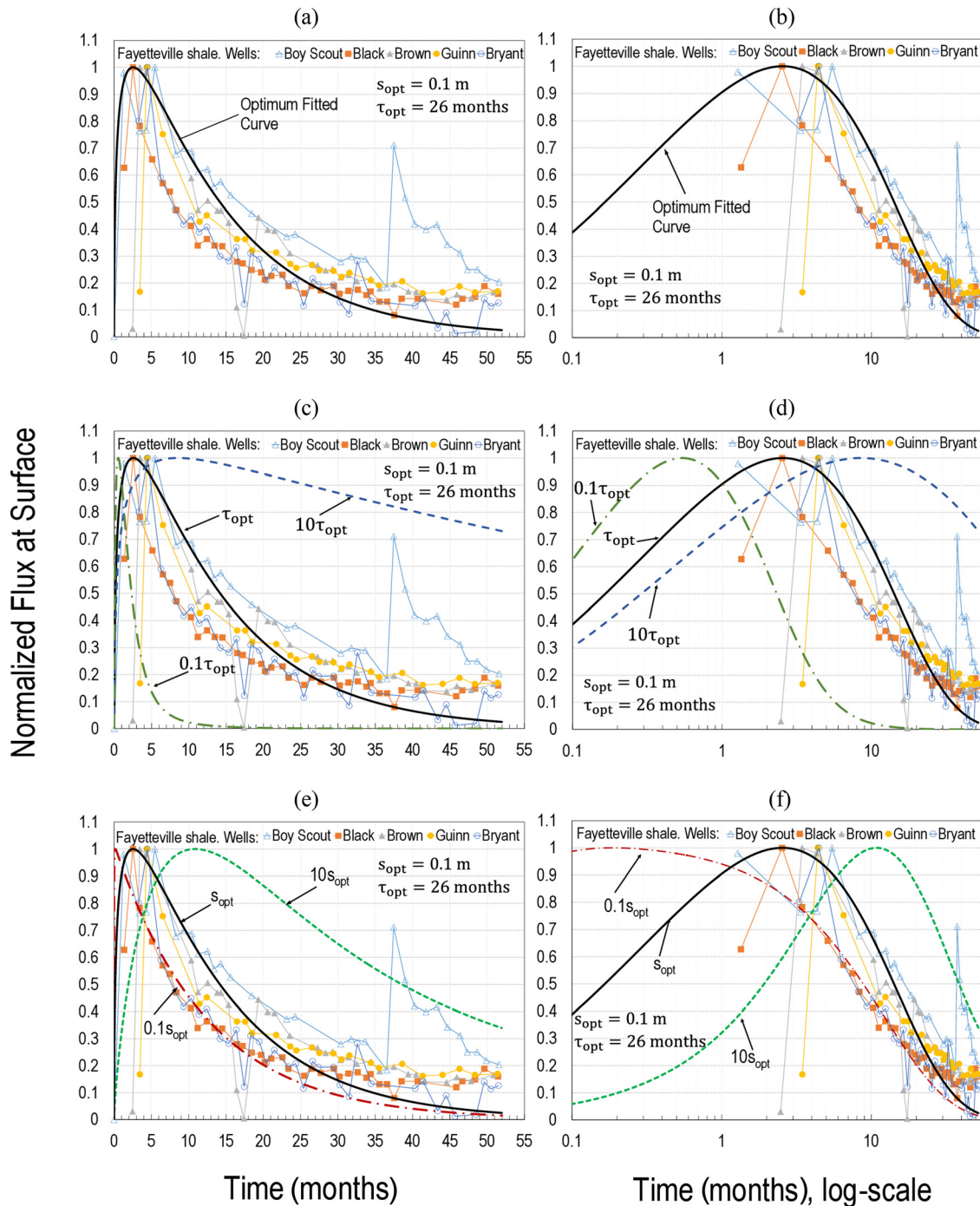

Fig. 4 Histories of gas flux at the surface observed at five different sites of Fayetteville shale [25], in actual and logarithmic time scales. Top row: curves of optimum fits; middle row: curves when characteristic delay time τ is changed; bottom row: curves when the crack spacing s is changed

permeability $k = 10^{-21}$ m^2, shale compressibility $C_s = 10^{-9}$ Pa^{-1}, initial pore pressure in shale $p = 25 \times 10^6$ Pa, and pressure at the surface $p_a = 10^5$ Pa.

To clarify the effect of permeability, a similar analysis has been done with k increased 10-fold, i.e., $k = 10^{-20}$ m^2. The optimum fit for this case was again good and provided $s_{opt} = 0.5$ m and $\tau_{opt} = 23$ months. Evidently, a realistic determination of permeability is very important.

What is the error of these estimates? To appraise it, the computations were further run with $s = s_{opt}$ but $\tau = 10 \tau_{opt}$ and $\tau = 0.1 \tau_{opt}$. As seen in Figs. 4(c) and 4(d), the calculated curves are totally out of the range of observations, both for the rate of decay and for the time to peak flow. Then the computations were run with $\tau = \tau_{opt}$ but $s = 10 s_{opt}$ and $0.1 s_{opt}$. As seen in Figs. 4(e) and 4(f), the increased spacing, which would be 1 m, is totally out of range. The curve for spacing of $0.1 s_{opt}$ is at the margin of long-term decay but the time to peak flow is too short by an order of magnitude, which is blatant in the log-time plot (Fig. 4(f)).

So it may be concluded that the expected errors of our average estimates are much less than an order of magnitude, probably not exceeding the factor of 2 or 1/2.

Questions may be raised with regard to the network of pre-existing joints and cracks, which have not been addressed specifically. All or most of them are filled and cemented by calcite and, whether or not filed, the overburden and tectonic pressures are so high that no open gaps can exist in these cracks. So they can provide no natural conduits for gas escape, unless opened by fracking fluid pressure. But the mechanics of this opening is not very different from hydraulic crack formation, as clarified later.

5 How to Achieve Dense Enough Spacing of Hydraulic Cracks

5.1 Review of Stability of Parallel Crack Systems. In the mid-1970 s, extensive studies of extracting heat from hot dry rock located relatively close to the earth surface were conducted. It was speculated that if a large vertical crack was created hydraulically from a borehole in hot granite and was then intersected by another borehole, circulation of water could deliver enough steam to generate electricity, like in geothermal basins with natural circulation [26]. Because of rapid decay of the heat conduction flux from a hot wall, success would have required many closely spaced parallel cooling cracks to propagate to a long distance from the walls of the large vertical crack. However, drilling into the giant Valles Caldera in the Jemez Mountains of New Mexico gave a negative result and studying the localization instability of parallel cooling cracks explained why. Nevertheless, this negative result provides today a valuable lesson for the fracking process.

Consider a system of interacting cracks of lengths $a_1, a_2, ..., a_N$ in a cooled (or shrinking) solid with fracture energy, Γ, and assume applicability of the linear elastic fracture mechanics (LEFM). The Helmholtz free energy has the general form

$$\mathcal{F} = U(a_1, a_2, ..., a_N; p) + \sum_{i=1}^{N} \int \Gamma \mathrm{d}a_i \quad (10)$$

where $U =$ strain energy of the elastic solid; $p =$ control parameter, such as the depth of penetration D of the cooling front into the halfspace (or, in our case considered later, the fluid pressure at the surface of halfspace). There are many possible fracture equilibrium solutions but thermodynamics requires the system to evolve in such a way that $\mathcal{F}$ be minimized. The problem is to determine which solution is stable and which solutions are unstable or metastable. The stable solution is what will occur.

The equilibrium and stability of the crack system are, respectively, decided by the first and second variations [27]

$$\delta \mathcal{F} = \sum_{i=1}^{m} \left(\frac{\partial U}{\partial a_i} + \Gamma \right) \delta a_i + \sum_{j=m+1}^{n} \left(\frac{\partial U}{\partial a_j} \right) \delta a_j \quad (11)$$

$$\delta^2 \mathcal{F} = \frac{1}{2} \sum_{i=1}^{n} \sum_{j=1}^{n} \left(\frac{\partial^2 U}{\partial a_i \partial a_j} \right) \delta a_i \delta a_j = \frac{1}{2} \sum_{i=1}^{n} \sum_{j=1}^{n} \mathcal{F}_{,ij} \delta a_i \delta a_j \quad (12)$$

(where a unit width b of the crack front is considered); here $i = 1, ..., m$ are the cracks that are propagating ($\delta a_i > 0$), dissipating fracture energy Γ; $i = m + 1, ..., n$ are the cracks that are shortening ($\delta a_i < 0$), for which the fracture energy is 0, and $i = n + 1, ..., N$ are the cracks that are immobile ($\delta a_i = 0$), which is a state that occurs when the energy release rate $-\partial \mathcal{U}/\partial a_i$ is nonzero but less than critical.

Equilibrium (or static) crack propagation requires vanishing of the first parenthesized expression in Eq. (11), which represents the Griffith crack propagation criterion of LEFM. There exist many equilibrium solutions, reachable along a stable equilibrium path. Fracture stability requires the matrix of $\mathcal{F}_{,ij}$, equal to $U_{,ij}$, to be positive definite, i.e.,

$$\det U_{,ij} > 0 \quad \text{and} \quad U_{11} > 0 \quad (13)$$

for the vectors of admissible variations δa_i [27,28–32] (note that $U_{,ij} = 2K_i K_{i,j}/E' = 2K_j K_{j,i}/E'$ where $K_i =$ stress intensity factor).

The admissible crack length variations δa_i are those satisfying the following restrictions:

$$\text{for} \quad -\partial U/\partial a_i = \Gamma : \quad \delta a_i \geq 0 \quad (14)$$

$$\text{for} \quad 0 < -\partial U/\partial a_i < \Gamma : \quad \delta a_i = 0 \quad (15)$$

$$\text{for} \quad \partial U/\partial a_i = 0 : \quad \delta a_i \leq 0 \quad (16)$$

In the special case of a parallel system of pre-existing natural cracks that are open up to length a_j but closed beyond, the effective fracture energy at the tip of open crack segment is 0 for both extension and shortening, i.e.,

$$\text{for} \quad \partial U/\partial a_j = 0 : \quad \text{any} \ \delta a_j \quad (17)$$

5.2 Localization Instability of Cooling Cracks and Hydrothermal Analogy With Pressurized Hydraulic Cracks. Consider a homogeneous elastic halfspace cooled by heat conduction. This produces a temperature profile in the form of the complementary error function, often approximated by a parabola, whose front advances into the halfspace as $\sqrt{t}$. The thermal stress, proportional to the temperature drop, is considered to produce an advancing system of parallel cooling cracks of equal spacing s, whose lengths are considered to alternate between a_1 and a_2. The crack lengths are assumed to be initially equal, $a_1 = a_2$ (although in reality the crack lengths, as well as spacings, are randomly distributed).

The positive definiteness of the matrix of $\mathcal{F}_{,ij}$ is first lost by the vanishing of $\det \mathcal{F}_{,ij}$. But this signifies neither instability nor bifurcation because the corresponding eigenvector $(\delta a_1, \delta a_2)$ implies every other crack to shorten ($\delta a_2 = -\delta a_1 \neq 0$), which is impossible since the energy release rates $-U_{,i}$ (or stress intensity factors K_i) of all cracks are nonzero ($K_i = \sqrt{E' U_{,i}}$); $E' =$ elastic modulus for plane stress (since the ground can lift, the plane stress is probably closer to reality than the plane strain). An exception is the opening of preexisting (noncemented, nonsticking) cracks, whose critical energy release rate can be zero; but, as pointed out later, this makes little difference.

After further crack growth, when the crack length is about $1.5 s$ to $2 s$ (depending on ratios s/D and l_0/D where $l_0 =$ Irwin's characteristic length), the positive definiteness of the matrix is lost due to the vanishing of $\mathcal{F}_{,11}$ (and $\mathcal{F}_{,22}$). The corresponding eigenvector $(\delta a_1, \delta a_2)$ has $\delta a_2 = 0$, which is admissible. It implies a stable bifurcation, in which one set of alternating cracks continues to grow ($\delta a_1 > 0$), while the remaining cracks get arrested ($\delta a_2 = 0$). The spacing of the leading cracks a_1 doubles, and their opening width w eventually doubles, too. Later, after further
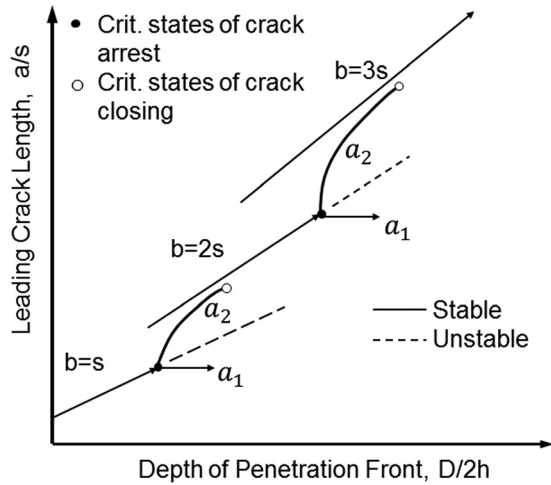
Fig. 5 Path of the lengths of thermal cooling cracks in the crack length space, adapted from Ref. [26]

Fig. 7 Leading crack length as a function of the depth of penetration front, for different temperature profiles along the cracks, adapted from Ref. [26]
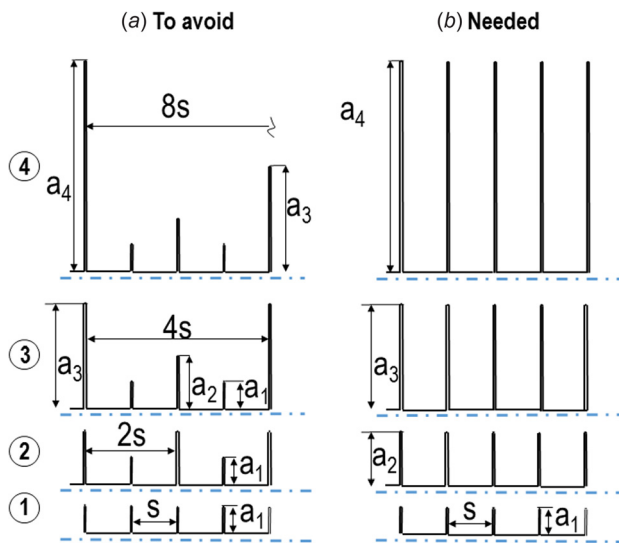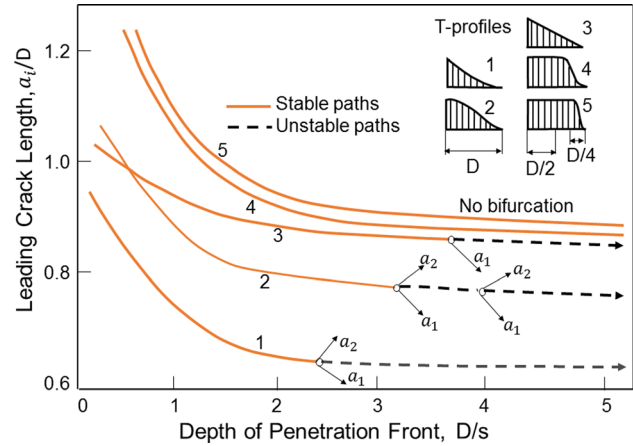

Fig. 6 Schematic representation of fracturing behavior (a) with crack localization—undesirable, and (b) without crack localization—desirable (prevention of localization greatly increases the percentage of gas that can be reached from the shale stratum by hydraulic fracturing)
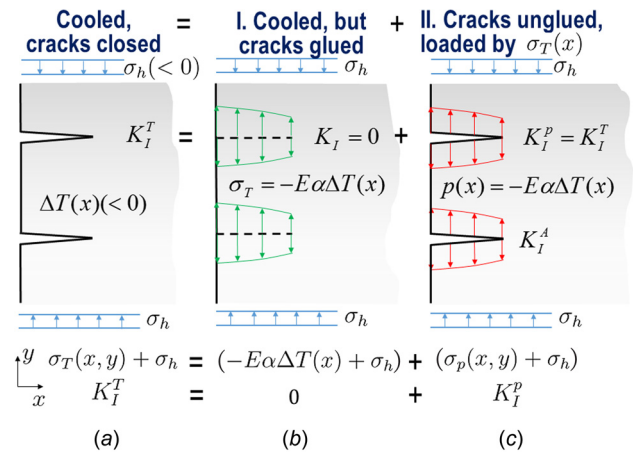

Fig. 8 Analogy of thermal and hydraulic cracks. The formation of the cooling cracks (a) can be decomposed into two steps: in the first step (b) the cracks are imagined to be glued so as to be kept closed. In the second step (c), the cracks are imagined to be unglued and allowed to open.

growth of a_1, cracks a_2 reduce their energy release rate to 0 and close [26,27,32].

The remaining leading, cracks, with spacing $2s$, eventually reach another bifurcation of the same kind, at which every other crack stops growing and gradually closes while the spacing of open cracks doubles to $4s$ (see Fig. 5), with eventual doubling of the opening width. This doubling of crack spacing, in which the crack system localizes into fewer and fewer cracks, is periodically repeated as the cooling advances; see [Refs. 28–30, Sec. 12.5]). Consequently, cooling of the rock by heat conduction cannot reach most of the rock mass (see Fig. 6). This fact is what killed the hot dry rock geothermal energy project as conceived in the 1970 s.

With regard to fracking, it is interesting to recall the 1970 s study of the effect of various temperature profiles along the cracks, which could conceivably be altered by heat convection in water flowing along the cracks; see Fig. 7, which shows, for several temperature profiles [28–30,33], the equilibrium curves of crack length versus the cooling front depth. The solid parts of the curves represent stable equilibrium states and the dashed parts

unstable equilibrium states. They are separated by the circle points, which indicate bifurcation states at which fracture localizes and every second crack stops growing.

As the temperature profile gets more uniform over a greater portion of crack depth, the bifurcation states are pushed to a greater crack depth. Eventually, for the profiles marked as 4 and 5, which have a long uniform portion and a steep or very steep temperature drop at the end, there is no bifurcation [33]. So, if such a temperature profile could be produced, the parallel cooling cracks would grow at constant spacing indefinitely.

5.3 Equivalence of Localization of Cooling Cracks and Pressurized Cracks. It is now interesting to point out that the previous analysis of cooling cracks can be easily transferred to fracking, which is a point that has apparently gone unnoticed. To explain, the situation in the left column of Fig. 8 shows an array of cooling cracks propagating from the surface of a halfspace, opened by temperature drop $\Delta T(x)$ which is assumed to depend only on depth coordinate x. The thermal stress field is denoted as $\sigma_T(x, y)$ (positive for tension). The halfspace is at the same time under tectonic pressure σ_h in the y direction normal to the surface (negative for compression). The stress intensity factor of the cooling cracks is denoted as K_I^T.

The formation of the cooling cracks (left column) can be decomposed into two steps:

(1) In the first step (middle column), the cracks are imagined to be glued so as to be kept closed. In that case the temperature field together with the tectonic stress S_h produces, along each cross section $y = 0$, normal stresses $\sigma^T(x) + \sigma_h$ where $\sigma^T(x) = -E'\alpha\Delta T(x)(\Delta T(x) \leq 0)$; here α is the thermal expansion coefficient and E' is the effective elastic modulus for plane strain of the rock. The rock is considered, for simplicity, as isotropic, although a generalization to orthotropic rock would not be difficult. The temperature drop ΔT is assumed to be big enough for the tensile thermal stress $\sigma^T(x)$ to overcome the tectonic stress. Since the cracks do not open, the stress intensity factor in this case vanishes, $K_I = 0$.

(2) In the second step (right column), the cracks are imagined to be unglued and allowed to open. This is equivalent to applying onto the crack faces pressure $p(x) = -\sigma_T(x)$ that is equal to the stress previously transmitted across the glued cracks (p is positive for compression). The stress intensity factor produced by this pressure is denoted as K_I^p. The stress field due to pressure on the cracks is denoted as $\sigma_p(x, y)$. The total stress field is $\sigma_p(x, y) - \sigma_h$. So,

$$p(x) = -E'\alpha\Delta T(x) \quad (p(x) \geq 0 \text{ assumed}) \tag{18}$$

$$K_I^p = K_I^T \tag{19}$$

The singular stress field of the cooling cracks is thus decomposed as $\sigma_T(x, y) = \sigma_T(x) + \sigma_p(x, y)$, and so the singular stress field due to pressurizing the unglued cracks may be expressed as

$$\sigma_p(x, y) = \sigma_T(x, y) + E'\alpha\Delta T(x) \tag{20}$$

onto which the tectonic stress $-\sigma_h$ gets superposed (see Fig. 8).

The foregoing hydrothermal equivalence of thermal and pressurized cracks can be extended to crack systems of different topology and geometry, e.g., with curved and variously inclined cracks. On the other hand, applicability is limited to the case of LEFM, in which the fracture process zone (FPZ) is assumed to be a point. In quasi-brittle fracture mechanics, the foregoing hydrothermal equivalence is only approximate. The reason is that the FPZ, considered to have a finite size, is affected by the nonsingular part of stress field, which is different in the left and right columns of Fig. 8.

The foregoing studies have been conducted without specifically considering that the cracks preferentially grow along the plentiful natural cracks or joints. Although their detailed consideration will require numerical simulation, qualitatively the same localization behavior must be expected. Closed or filled naturally cemented cracks do not change significantly the stiffness characteristics of the shale mass. When a crack propagates along a weak, naturally cemented, preexisting crack or joint, the only significant difference is that the fracture energy is smaller, perhaps even zero, as discussed later. But this does not change our conclusions about localization qualitatively.

So we may conclude that the effect of temperature profile on fracture propagation is generally the same as that of a similar crack pressure profile. Thus the previous analysis of cooling cracks makes it possible to state, even without any calculations, that by achieving a sufficiently uniform crack pressure profile, with a sufficiently steep pressure front, the parallel cracks should not get localized and should propagate indefinitely, at constant spacing. This is what is needed to create densely spaced channels by which the shale gas could escape from the nanopores.

Since the fracking actually works, we must conclude that such pressure profiles are indeed being achieved to a significant degree, though not within more than 15% of the volume of shale stratum.

It is intuitive that it is mainly a matter of pumping rate and history (surely also influenced by proppants and gelants). If the pressure at crack mouth were increased in small steps and after each step the pressure was held constant long enough, the pressure in the cracks would eventually become uniform (however, since there is extensive leaking of the fracking fluid into pores and voids other than the cracks, the pumping rate must be corrected for the leaking and what matters is the rate of fluid influx at the crack mouths).

5.4 Numerical Results on Localization of Fluid Pressurized Cracks. The foregoing analysis applies to the plane strain situation, which is a reasonable approximation for vertical cracks spreading widely from the horizontal borehole and over the full depth of the stratum. In an earlier stage (though not right at the start of cracks from the casing perforated in one direction only), these cracks are probably better approximated as circular cracks. Then the problem is approximately axisymmetric.

To examine the broader validity of the foregoing inferences from thermal stress analogy in plane strain situation, axisymmetric finite elements are now used to analyze the stability of a system of primary vertical circular cracks of equal spacing s (Fig. 9), normal to the direction of perforated horizontal borehole. This is, of course, a simple idealization of cracks which are surely quite irregular and may propagate preferentially along pre-existing cemented joints. Also, for the sake of simple illustration, we treat the shale as isotropic, knowing that the orthotropy of shale would have to be taken into account for more realistic prediction. The response is assumed to be symmetric with respect to each crack plane, which is again an idealized situation obtained for a crack system infinite in the direction normal to the cracks. For numerical reasons, the body containing the cracks is assumed to be an infinite cylinder with the borehole in the axis. Then it is possible to exploit symmetry with respect to the crack planes and analyze only a slice of the cylinder between two crack planes. The cylinder radius $R = 60s$, is considered sufficiently larger than the crack radius.
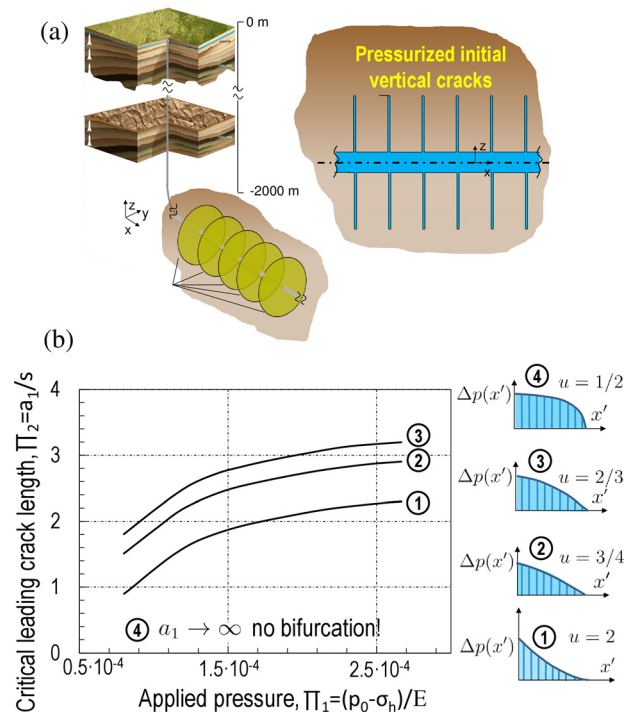

Fig. 9 (*a*) Idealized circular hydraulic cracks around a horizontal borehole considered for simple analysis of localization instability (not to scale) and (*b*) dimensionless critical crack lengths as a function of dimensionless applied pressure $\Pi_1 = (p_0 - \sigma_h)/E$ for different hydraulic pressure profiles shown. The results show that nearly uniform pressure profiles prevent localization.

The tectonic minimum principal stress, which is normal to the cracks, is considered to be $\sigma_h = 40$ MPa. The shale is simplified as isotropic, with Young's modulus $E = 37,500$ MPa, Poisson ratio $\nu = 0.3$, and fracture energy $G_f = 208$ J/m^2. It is assumed that crack radii alternate as a_1, a_2 as shown in Fig. 9, and that initially $a_1 = a_2$. The pressure, p_0, of the fluid in the borehole is gradually raised to extend the cracks and various dimensionless pressure profiles along the radius are assumed to be maintained the same during the crack growth, given by the equation

$$\Delta p(x') = \left(1 - \frac{x'}{D}\right)^u (p_0 - \sigma_h) \qquad (21)$$

From the results of the bifurcation analysis, plotted in Fig. 9, two observations can be made

(1) If the stability of the dense crack system is not unlimited, an increase of the pressure applied from the borehole tends to increase the critical crack length at bifurcation and thus tends to stabilize the distributed crack system, i.e., prevent crack closing and localization into one crack.

(2) For the pressure profiles with a mild pressure decrease over the crack length and a steep pressure drop near the crack tip ($u = 1/2$ or $3/4$, top of Fig. 9), the crack system path exhibits no bifurcation in the (a_1, a_2) space, and maintains the original crack spacing and equal crack length ($a_1 = a_2$) indefinitely, without localization.

Aside from favorable crack pressure profiles, addition of proppants (fine sand) and acids to the fracking water are other empirically introduced measures that have been proven to help fracking. It is generally considered that their purpose is to keep the cracks open during gas extraction. But not only that. The present analysis shows that the proppants are also important for preventing or partially limiting crack localizations during the hydraulic fracturing process.

Why have the acids been found to help gas extraction? This is also unclear from the mechanics viewpoint. We speculate that the acids help to loosen the asperities from the crack walls, thus creating fragments and debris that tend to keep the cracks open during gas extraction. But again, like the proppants, this not the only role of acids. Their another role may be partial prevention of crack localizations by producing more fragments in the cracks.

For a fixed profile, the crack system bifurcation problem involves five variables: E, Γ, p, s, a_1. Since they involve only 2 independent dimensions, length and force, the solution must depend (according to the Vashy–Buckingham theorem of dimensional analysis) on only 3 dimensionless parameters. They are

$$\Pi_1 = \frac{p_0 - \sigma_h}{E}, \quad \Pi_2 = \frac{a_1}{s}, \quad \Pi_3 = \frac{s}{l_1} \quad \left(l_1 = \frac{\Gamma}{E}\right) \qquad (22)$$

where $\Pi_1 =$ dimensionless crack pressure, $\Pi_2 =$ dimensionless leading crack length, $\Pi_3 =$ dimensionless crack spacing and $l_1 =$ characteristic crack spacing. In the cooling problem, there is always one more parameter $\Pi_4 = D/s$ where D is the cooling front depth; and here, too, there is parameter $\Pi_4 = x/a_1$. Mapping of all possible solutions in terms of these parameters is relegated to future work. For dense cracks of small enough spacing s (and also for a larger scale model with smeared joints), the tensile strength of shale, f_t, must also matter, in the sense of the cohesive crack model, and then there is an additional dimensionless parameter $\Pi_5 = l_0/s$ where $l_0 = E\Gamma/f_t^2 =$ Irwin's characteristic length for cohesive (or quasi-brittle) fracture.

5.5 Localization in Pre-Existing System of Natural Cracks or Rock Joints. The shale mass typically contains one or several systems of nearly parallel pre-existing natural cracks or joints. Their typical spacing ranges from 0.1 m to 1 m. Due to tectonic and overburden pressures, the opposite faces are in perfect contact and so these opposite cracks and joints cannot serve as conduits for fluid unless opened up by high enough pressure of the fracking fluid.

Often these natural cracks are filled and cemented by calcite or other minerals. So, their opening requires a finite fracture energy Γ, which may be expected to be smaller than the Γ of the intact shale. Then, if they are normal or nearly normal to the minimum principal stress, the fracking fluid will open them first. Their behavior, including localization, is similar to new cracks in intact rock.

Some natural cracks might not be cemented by a fill, in which case their fracture energy $\Gamma = 0$. Does that make such natural crack system more likely, or less likely, to serve as conduits for extracting gas?—Little less likely, because the natural cracks, while easier to open, are slightly more prone to localization.

The bifurcation state that indicates localization is determined by the vanishing of the second variation $\delta^2 \mathcal{F}$ (Eq. (11)), which is independent of whether Γ is finite or zero. However, there is a difference in the admissibility of the eigenvector through which the matrix of $\mathcal{F}_{,ij}(i, j, = 1, 2)$ loses positive definiteness (Eq. (13), $\mathcal{F}_{,ij} = U_{,ij}$). As pointed out before, the singularity occurs first through the vanishing of the determinant of $\mathcal{F}_{,ij}$. The corresponding eigenvector, $(\delta a_1, \delta a_2) \propto (1, -1)$ [28–30], is, in view of Eqs. (14)–(16), inadmissible for new cracks because their energy release rate $-U_{,i}$ is nonzero.

However, for uncemented natural cracks such an eigenvector is, according to Eq. (17), and in absence of proppants admissible, i.e., every other crack can start shortening as the others extend (the closed crack portion is not counted into the crack length). So for natural cracks, for which $\Gamma = 0$, the localization of parallel cracks will occur earlier in the fracking process than it will for parallel cracks with $\Gamma > 0$ in intact rock, in which those cracks localize only later, after $\mathcal{F}_{,11}$ vanishes (Eq. (13)), with $(\delta a_1, \delta a_2) \propto (1, 0)$.

5.6 Hierarchical Refinement of Hydraulic Crack System. A possible idealized picture of crack system development may now be offered. From the horizontal borehole, the first vertical cracks, orthogonal to the borehole, must form at the locations of casing perforations. In reality, these primary cracks are sure not to be exactly planar nor exactly vertical, nor exactly circular, since they should preferably follow the irregular near-vertical rock joints.

Then, in the direction roughly normal to the larger principal tectonic stress σ_H, one can imagine formation of a system of secondary vertical cracks of denser spacing, roughly orthogonal to the primary vertical cracks. These cracks may form again preferentially following the rock joints or slip faults of roughly that direction. They would likely start by fluid penetration into the rock inhomogeneities such as faults, joints, and pre-existing cracks, driven by horizontal tensile stress parallel to the to the primary crack walls, produced by expansion of the fracking zone under fluid pressure. If a nearly uniform pressure profile with a steep front can be maintained in these secondary cracks, they are likely not to localize and thus maintain their narrow spacing (Fig. 10).

It is thus clear that, to explain the known percentage of gas extraction, a hierarchical multilevel crack system that leads to fine cracks with the spacing of about 0.1 m must get formed. Since the initiation of cracks from a smooth surface is governed, according to the cohesive crack model, by the tensile strength rather than the fracture energy, tensile stresses parallel to the walls of the higher-level crack must develop. These horizontal tensile stresses must be generated as a reaction to the pressurization of a large enough volume of the fracturing zone in shale. In similarity to what is known for concrete, the initial spacing of the sublevel cracks produced by tensile stress along the wall of a higher-level crack is expected to be roughly equal to the spacing of shale inhomogeneities, which is also the spacing of weak spots on the wall.

Although the nearly horizontal bedding planes have the lowest fracture energy, the cracks cannot follow these planes except if the fluid pressure exceeds the overburden pressure. Branching at acute angles at the crack tip is unlikely because one pressurized branch would shield the other (branching does occur at dynamic propagation of cracks running at nearly the Raleigh wave speed, but the overall fracking process, taking several days, is static
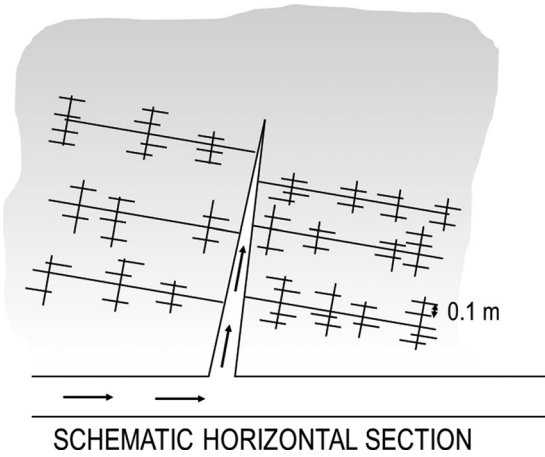
Fig. 10 Schematic horizontal section showing how a hierarchical refinement of hydraulic crack system may lead to crack spacing of about 0.1 m

except that local sound-generating dynamic crack jumps occur, due to inhomogeneities).

6 The Intriguing Prospect of Comminuting Shale Near Borehole by Shock Waves

Recent years have seen a revival of the idea to stimulate gas release from shale by shock waves emitted by explosions in the horizontal borehole. Oil companies have been experimenting with various types of explosions in the borehole, including electric pulsed arc [34,35]. Although preliminary studies show that shock waves from explosions could comminute the shale only in a zone much smaller than the thickness H of the shale stratum, shock waves could nevertheless help locally in the vicinity of the borehole.

The shock waves would comminute the compressed shale by high rate shear. To simulate it computationally, a theory inspired by analogy with turbulence has recently been conceived [36,37]. At high shear rates, the driving force of comminution under triaxial compression is not the release of strain energy, as in classical fracture mechanics, but the release of the local kinetic energy of shear strain rate of particles being formed by interface fracture. It transpired that at shear strain rates $>10^4/s$, the local kinetic energy density exceeds the maximum possible strain energy density (i.e., the density at the strength limit) by several orders of magnitude.

Since the formulation involves quantities with both the stress or energy density (dimension J/m^3) and surface energy (dimension J/m^2), there must exist a material characteristic length which governs the particle size (note that if particle breakage were attributed to exceeding the strength limit, the particle size would be zero). It is found that the particle size or crack spacing should be proportional to the $-2/3$ power of the shear strain rate, and that the comminution process is macroscopically equivalent to an apparent shear viscosity proportional to the $-1/3$ power of the shear strain rate. A dimensionless indicator of the comminution intensity was formulated. The theory was inspired by noting that the local kinetic energy of shear strain rate plays a role analogous to the local kinetic energy of eddies in turbulent flow.

7 Key Points and Conclusions

(1) So what makes fracking work? It is: (a) the creation of a dense system of hydraulic cracks with the spacing of only about 0.1 m (for the typical permeability considered) and (b) the prevention or mitigation of the localization instabilities of parallel crack systems.

(2) If the permeability of shale along the bedding layers is known, the spacing of hydraulic cracks can be estimated

from: (a) the history of gas flux on the surface and (b) the terminal percentage of gas extracted from the shale stratum (which has been only about 15% or less).

(3) To this end, a good estimate requires a computer program simulating (a) the gas diffusion from shale layer into parallel cracks and (b) the flow of gas bubbles through the hydraulic cracks and the pipes.

(4) The key features of flux history whose optimal matching yields the crack spacing are two: (a) the half-time of flux rate decay and (b) the time to reach the peak flux rate.

(5) In LEFM, the problems of pressurized cracks and cooling cracks are perfectly analogous. Whether or not a hydraulic crack system would localize into sparse wide cracks can be easily inferred from the previous studies of cooling cracks (or shrinkage cracks in concrete). For cohesive cracks, this hydrothermal analogy is only approximate. The smaller the fracture process zone compared to the crack spacing, the better is the hydrothermal analogy.

(6) The key to preventing localization is to achieve and maintain a sufficiently uniform pressure profile, with a sufficiently steep pressure drop at front. This calls for sufficiently slow rise of pressure at the point of fluid injection from the perforated casing into the shale mass, which can be controlled by the pumping rate, corrected for leaks, as well as by changes of fluid viscosity and the type and concentration of proppants.

(7) Aside from the pressure profile, the proppants also help to prevent or mitigate crack localization instabilities. So do the fragments created by loosening of asperities from crack walls (which might be promoted by acids in the fracking fluid). However, the proppant or fragments can be only partially effective against localizations since they cannot prevent partial closing of cracks wider than the grain or fragment size.

(8) While the pre-existing uncemented (unfilled) natural cracks or joints are easier to open, they are more prone to localization and thus are unlikely to be of much help in achieving the afore-mentioned dense crack spacing.

(9) Computer simulation of hypothetical crack evolution and pressure profiles based on pumping history may be expected to help in optimizing the fracking process.

(10) Increasing the densely fractured volume with many narrow cracks, at the expense of sparsely fractured volume with few wide cracks, will also provide environmental benefits because it will reduce the flowback of contaminated water per m^3 of gas.

8 Remark on Broader Benefits

Another environmental benefit is a reduction of maximum seismicity, because localization instabilities in inhomogeneous rock can be dynamic and also because in denser crack systems the dynamic crack extensions tend to be shorter. The suppression of cracking localization may benefit even more the underground sequestration of CO_2 and other fluids, which is done from vertical boreholes, is more prone to crack localization and produces higher seismicity than fracking.

Acknowledgment

Appendix

Expansion of Pressurized Elliptic Hole in Infinite Plane

Linear elasticity is assumed, and thus superposition can be used to analyze a hole pressurized internally by pressure p_f equal to the difference between the fluid pressure and the average tectonic pressure (Fig. 3(c)). It is convenient to introduce the elliptic coordinates ξ and η defined by the following conformal mapping:

$$z = c \cosh \zeta \quad \zeta = \xi + i\eta \tag{A1}$$

This gives

$$x = c \cosh \xi \cos \eta \quad y = c \sinh \xi \sin \eta \tag{A2}$$

where c = focal distance. On the ellipse, coordinate ξ is constant. The major and minor semi-axes are, respectively, $a = c \cosh \xi_0$ and $b = c \sinh \xi_0$. The stress, strain, and displacement fields can be described by the following two potentials [24]:

$$\psi(z) = \frac{p_f c}{2}(\sinh \zeta - \cosh \zeta) \quad \chi(z) = -\frac{p_f c^2}{2} \zeta \cosh 2\xi_0 \tag{A3}$$

which can be used to calculate the cartesian displacements as $u_x + iu_y = 1/2G[(3 - \nu^*)/(1 + \nu^*)\psi(z) - z\bar{\psi}'(\bar{z}) - \bar{\chi}'(\bar{z})]$ where G = shear modulus of shale, $\nu^* = \nu/(\nu + 1)$ for plane strain, and $\nu^* = \nu$ for plane stress (closer to present situation) [38]. After some algebraic manipulations the displacement field under plane stress can then be described by the following simple equations:

$$u_x = \frac{p_f c \sinh \xi \cos \eta}{2G(1 + \nu)} \frac{\Pi(\xi, \eta) - (1 - \nu)\coth \xi}{\cosh 2\xi - \cos 2\eta} \tag{A4}$$

$$u_y = \frac{p_f c \cosh \xi \sin \eta}{2G(1 + \nu)} \frac{\Pi(\xi, \eta) - (1 - \nu)\tanh \xi}{\cosh 2\xi - \cos 2\eta} \tag{A5}$$

$$\Pi(\xi, \eta) = (1 - \nu)\cosh 2\xi + (1 + \nu)\cosh 2\xi_0 - 2\cos -2\eta \tag{A6}$$

To compute the area change, it is now convenient to find displacement u_ξ which is the displacement in the direction orthogonal to the curve $\xi = \xi_0$. This can be easily found by noting that $u_\xi + iu_\eta = e^{-i\alpha}(u_x + iu_y)$ in which α can be defined by $e^{2i\alpha} = \sinh \zeta / \overline{\sinh \zeta}$. The result is

$$u_\xi = \frac{u_x \sinh \xi \cos \eta + u_y \cosh \xi \sin \eta}{\sqrt{1/2(\cosh 2\xi - \cos 2\eta)}} \tag{A7}$$

Taking advantage of symmetry, one can easily calculate the area change of the ellipse $\xi = \xi_0$

$$\Delta A = 4 \int_0^{\pi/2} u_\xi(\eta) c \cosh \xi_0 \, d\eta \tag{A8}$$

References

[1] Beckwith, R., 2010, "Hydraulic Fracturing: The Fuss, the Facts, the Future," J. Pet. Technol., **62**(12), pp. 34–41.

[2] Montgomery, C. T., and Smith, M. B., 2010, "Hydraulic Fracturing: History of an Enduring Technology," J. Pet. Technol., **62**(12), pp. 26–32.

[3] Society of Petroleum Engineers, 2010, *Legends of Hydraulic Fracturing*, (CDROM), Society of Petroleum Engineers, Richardson, TX.

[4] Adachi, J. I., and Detournay, E., 2008, "Plane Strain Propagation of a Hydraulic Fracture in a Permeable Rock," Eng. Fract. Mech., **75**(16), pp. 4666–4694.

[5] Gale, J. F. W., Reed, R. M., and Holder, J., 2007, "Natural Fractures in the Barnett Shale and Their Importance for Fracture Treatments," AAPG Bull., **91**(4), pp. 603–622.

[6] Bažant, Z. P., Salviato, M., and Chau, V. T., 2014, "Why Fracking Works and How to Optimize It," Department of Civil and Environmental Engineering, Northwestern University, Evanston, IL, Report No. 14-06/008w.

[7] Cipolla, C. L., Mayerhofer, M. J., and Warpinski, N. R., 2009, "Fracture Design Considerations in Horizontal Wells Drilled in Unconventional Gas Reservoirs,"

[8] Rijken, P., and Cooke, M. L., 2001, "Role of Shale Thickness on Vertical Connectivity of Fractures: Application of Crack-Bridging Theory to the Austin Chalk," Tectonophysics, **337**(1–2), pp. 117–133.

[9] Haifeng, Z., Hang, L., Guohua, C., Yawei, L., Jun, S., and Peng, R., 2013, "New Insight Into Mechanisms of Fracture Network Generation in Shale Gas Reservoir," J. Pet. Sci. Eng., **110**, pp. 193–198.

[10] Ajayi, B., Aso, I. I., Terry, I. J., Walker, K., Wutherich, K., Caplan, J., Gerdom, D. W., Clark, B. D., Gunguly, U., Li, X., Xu, Y., Yang, H., Liu, H., Luo, Y., and Waters, G., 2013, "Stimulation Design for Unconventional Resources," Oilfield Rev., **25**(2), pp. 34–46.

[11] Gale, J. F. W., 2002, "Specifying Lengths of Horizontal Wells in Fractured Reservoirs," SPE Reservoir Eval. Eng., **5**(3), pp. 266–272.

[12] Olson, J. E., 2004, "Predicting Fracture Swarms—The Influence of Subcritical Crack Growth and the Crack-Tip Process Zone on Joint Spacing in Rock," J. Geol. Soc. London, **231**, pp. 73–87.

[13] Louck, R. G., Reed, R. M., Ruppel, S. C., and Jarvie, D. M., 2009, "Morphology, Genesis, and Distribution of Nanometer-Scale Pores in Siliceous Mudstones of the Mississippian Barnett Shale," J. Sediment. Res., **79**(12), pp. 848–861.

[14] Javadpour, F., Fisher, D., and Unsworth, M., 2007, "Nanoscale Gas Flow in Shale Gas Sediments," J. Can. Pet. Technol., **46**(10), pp. 55–61.

[15] Javadpour, F., 2009, "Nanopores and Apparent Permeability of Gas Flow in Mudrocks (Shales and Siltstones)," J. Can. Pet. Technol., **48**(8), pp. 16–21.

[16] Maurel, O., Reess, T., Matallah, M., de Ferron, A., Chen, W., La Borderie, C., Pijaudier-Cabot, G., Jacques, A., and Rey-Bethbeder, F., 2010, "Electrohydraulic Shock Wave Generation as a Means to Increase Intrinsic Permeability of Mortar," Cem. Concr. Res., **40**(12), pp. 1631–1638.

[17] Soeder, D. J., 1988, "Porosity and Permeability of Eastern Devonian Gas Shale," SPE Form. Eval., **3**(1), pp. 116–124.

[18] Cui, X., Bustin, A. M. M., and Bustin, R. M., 2009, "Measurements of Gas Permeability and Diffusivity of Tight Reservoir Rocks: Different Approaches and Their Applications," Geofluids, **9**(3), pp. 208–223.

[19] Metwally, Y. M., and Sondergeld, C. H., 2010, "Measuring Low Permeabilities of Gas-Sands and Shales Using a Pressure Transmission Technique," Int. J. Rock Mech. Min. Sci., **48**(7), pp. 1135–1144.

[20] Guidry, K., Luffel, D., and Curtis, J., 1996, "Development of Laboratory and Petrophysical Techniques for Evaluating Shale Reservoirs: Final Technical Report, October 1986–September 1993," Gas Shale Project Area, ResTech, Inc., Houston, TX, GRI Contract No. 5086-213-1390, Report No. GRI-95/0496.

[21] API, 1998, *Recommended Practices for Core Analysis*, 2nd ed., American Petroleum Institute, Washington, DC, Recommended Practice 40.

[22] Adachi, J., Siebrits, E., and Peirce, A., 2007, "Computer Simulation of Hydraulics Fractures," Int. J. Rock Mech. Min. Sci., **44**(5), pp. 739–757.

[23] Bear, J., 1988, *Dynamics of Fluids in Porous Media*, American Dover Publications, Mineola, NY.

[24] Stevenson, A. C., 1945, "Complex Potentials in Two-Dimensional Elasticity," Proc. R. Soc. London, Ser. A, **184**(997), pp. 129–179.

[25] Mason, J. E., 2011, "Well Production Profiles Assess Fayetteville Shale Gas Potential," Oil Gas J., **109**(14), pp. 76–81.

[26] Bažant, Z. P., and Ohtsubo, R., 1978, "Geothermal Heat Extraction by Water Circulation Through a Large Crack in Dry Hot Rock Mass," Int. J. Numer. Anal. Methods Geomech., **2**(4), pp. 317–327.

[27] Bažant, Z. P., and Ohtsubo, H., 1977, "Stability Conditions for Propagation of a System of Cracks in a Brittle Solid," Mech. Res. Commun., **4**(5), pp. 353–366.

[28] Bažant, Z. P., and Cedolin, L., 1991, *Stability of Structures: Elastic, Inelastic, Fracture and Damage Theories*, Oxford University Press, New York.

[29] Bažant, Z. P., and Cedolin, L., 2003, *Stability of Structures: Elastic, Inelastic, Fracture and Damage Theories*, 2nd. ed., Dover Publications, Mineola, NY.

[30] Bažant, Z. P., and Cedolin, L., 2010, *Stability of Structures: Elastic, Inelastic, Fracture and Damage Theories*, 3rd ed., World Scientific, Singapore.

[31] Bažant, Z. P., Ohtsubo, R., and Aoh, K., 1979, "Stability and Post-Critical Growth of a System of Cooling and Shrinkage Cracks," Int. J. Fract., **15**(5), pp. 443–456.

[32] Nemat-Nasser, S., Keer, L. M., and Parihar, K. S., 1976, "Unstable Growth of Thermally Induced Interacting Cracks in Brittle Solids," Int. J. Solids Struct., **14**(6), pp. 409–430.

[33] Bažant, Z. P., and Wahab, A. B., 1979, "Instability and Spacing of Cooling or Shrinkage Cracks," J. Eng. Mech.-ASCE, **105**(5), pp. 873–889.

[34] Chen, W., Maurel, O., Reess, T., de Ferron, A., La Borderie, C., Pijaudier-Cabot, G., Rey-Bethbeder, F., and Jacques, A., 2012, "Experimental Study on an Alternative Oil Stimulation Technique for Tight Gas Reservoirs Based on Dynamic Shock Waves Generated by Pulsed Arc Electrohydraulic Discharges," J. Pet. Sci. Eng., **88–89**, pp. 67–74.

[35] Safari, R., Huang, J., Mutlu, U., and Glanville, J., 2014, "3D Analysis and Engineering Design of Pulsed Fracturing in Shale Gas Reservoirs," 48th U.S. Rock Mechanics/Geomechanics Symposium, Minneapolis, MN, June 1-4.

[36] Bažant, Z. P., and Caner, F. C., 2013, "Comminution of Solids Caused by Kinetic Energy of High Shear Strain Rate, With Implications for Impact, Shock and Shale Fracturing," Proc. Natl. Acad. Sci. U.S.A., **110**(48), pp. 19291–19294.

[37] Bažant, Z. P., and Caner, F. C., 2014, "Impact Comminution of Solids Due to Local Kinetic Energy of High Shear Strain Rate: I. Continuum Theory and Turbulence Analogy," J. Mech. Phys. Solids, **64**, pp. 223–235 (with Corrigendum, 2014, **67**, p. 14).

[38] Timoshenko, S., and Goodier, J. N., 1970, *Theory of Elasticity*, 3rd ed., McGraw-Hill, New York, Secs. 62, 63.